Check for
updates

The weakly non-linear waves propagation for Kelvin–Helmholtz instability in the magnetohydrodynamics flow impelled by fractional theory

Waqas Ali Faridi[1] · Muhammad Imran Asjad[1] · Adil Jhangeer[2] · Abdullahi Yusuf[3,4] · Tukur Abdulkadir Sulaiman[3,4]

Abstract

The weakly nonlinear wave propagation that occurs in the presence of magnetic fields, in which energy is concentrated in a narrow band of wave-numbers in a dispersive and dissipative fluid. The main objective of this paper is to analyze the $(2 + 1)$−dimensional elliptic nonlinear Schrodinger equation under the influence of three different fractional operators. The generalized fractional soliton solutions and propagation of magnetohydrodynamics fluid in sort of solition will be visualized. The Conformable, β and M-truncated fractional operator applied to classical evolution Schrodinger equation. In order to get the analytical closed form solution, one of the generalized approach new extended direct algebraic method is utilized. The fractional nonlinear elliptic Schrodinger equation is developed in three different fractional sense. The similarity transformation technique converted the controlling fractional system to ordinary differential equations. The fractional analytical solutions such as, plane solution, mixed hyperbolic solution, periodic and mixed periodic solutions, mixed trigonometric solution, trigonometric solution, shock solution, mixed shock singular solution, mixed singular solution, complex solitary shock solution, singular solution and shock wave solutions are obtained. The graphical 2-D and 3-D representation of the results is shown to express the propagation of fluid with the magnetic field by assuming the appropriate values of the involved parameters. The graphical performance of the obtained solution at various settings of parametric values and fractional order reveals new perspectives and fascinating model phenomena. The attained outcomes have significant applications and have opened up innovative development areas for research across numerous scientific fields.

Keywords New direct extended algebraic method · The weakly non-linear wave propagation theory with a magnetic field · Traveling wave solutions · Fractional differentiation

✉ Tukur Abdulkadir Sulaiman
   sulaiman.tukur@fud.edu.ng

Extended author information available on the last page of the article

1 Introduction

The complicated dynamical communication of real-world phenomena can be demonstrated in knowing how to deviate an occurrence in terms of space and time. The partial differential equation has the most distinguished legacy for displaying how a physical phenomena is happening in space and time. Any physical phenomenon involving partial differential equations must be approached with the fundamental concept of the instantaneous rate of change. The classical theory of differentiation is the magnificent concept in the modern fields to explain the complicated natural phenomenons in a consistent fashion. However, the fractional differential theory is employed to discover the physical properties of several significant natural systems and to improve the effectiveness of already-existing inaccessible processes. The fractional differential theory is an extension of the basic differentiation theory, where the classical theory of differentiation has a week singularity, the theory of fractional differentiation is conceivable.

The various production of fractional differential operators is novel. A few significant and highly practical fractional operators are shown here like, Riemann-Liouville derivative and modified version (Guy 2006), Caputo operator (Michele 1967), conformable differential operator (Roshdi et al. 2014), truncated-M derivative (Sousa and Oliveira 2017), β differential operator (Alwyn 2006), Caputo-Fabrizio derivative with non-singular kernel (Michele and Fabrizio 2015) and also Attangana-Baleanu in Caputo and R-L sense encompassing non-singular kernel (Atangana and Baleanu 2016). The fractional partial differential equations permit us to generalize the classic partial differential equations and also allows one to uncover the chemistry of physical events in a cavernously and far-reaching sense. The analytical findings of the alcohol concentration in the blood and the alcohol concentration in the stomach are assessed using the Sumudu transform method by Singh Jagdev (2020). The Banach fixed point theorem approach is used to establish the existence and uniqueness of the solution of the fractional Coronavirus model, which is formulated in the Atangana-Baleanu-Caputo derivative sense (Ebenezer et al. 2021). Jagdev et al. (2022) analyzed and developed the fractional soliton solutions of the fractional Caudrey-Dodd-Gibbon equation. Behzad et al. (2022) studied the local fractional longitudinal wave equation in a magneto-electro-elastic circular rod in fractal media.

The partial differential equation carries at least one dependent variable which usually interprets any physical entity such as the surface height of water waves or magnitude of electromagnetic waves in connection to time. An extensive range of scientific areas utilise non-linear partial differential equations to incorporate non-linearity to the partial differential equation (Agrawal 2013; Muhammad et al. 2017; Kimeu 2009; Abdeljawad 2015; Roger et al. 1988). The partial differential equations encompassing non-linearity have quite an influence in diverse areas of mathematical sciences, engineering fields, and applied sciences. The study and analysis of non-linear partial differential equations through solitonic wave solutions is certainly a magnificent objective for scientific interpretation. On the account of obtaining the exact wave solutions and for reporting the intricated non-linear systems in the non-linear sciences, non-linear partial differential equations through solitonic wave solutions are a splendiferous and elevated avenue for physicists and mathematicians. The analysis of the serpentine physical process on the account of solitons is a spectacular study. The non-linear Schrödinger equation has been anatomized through a solitonic perspective in outrageous aspects (Xue et al. 2019; Weitian et al. 2019; Xiaoyan et al. 2019; Helal and Seadawy 2009; Seadawy 2015).

In certain scenarios, the combination of two fluids forms an instability which is classed as Kelvin Helmholtz instability (KHI). The instabilities of such type have consequential contributions in astrophysics, physics of space, fluids flow, and plasma physics. Few examples of this can see seen in the dynamical process of the radioactive galaxies in the jet zone, the spiral galaxy hose (Blandford et al. 1982), the planetary stratiform atmosphere, the dynamical procedure of the magnetic rupture zone at the boundary (Parhi 1992), the common tail (Schilinski and Chernii 1987), the stability of the plasma cutting flow connecting the solar wind to the magnetosphere (Min et al. 1997), the interface among conterminous flows of heterogeneous speed in solar wind (Parker 1963). The inquisition of the non-linear saturation phase of the cross-field electrostatic (KHI) in plasma sturdily magnetized is being impelled by the experiments in the laboratory (Khater et al. 2001, 2006; Nielsen et al. 1992). The instability of in-homogeneous plasma flux in cross the electric and magnetic fields is a remarkable certain process (Wang et al. 1992). The geomagnetic space of earth has distinct waves in the upper ionosphere (Lindqvist et al. 1994) and the auroral area (Temerin et al. 1979). Wu and Wang analyzed the solitary wave structures and vindicated the practicability of prosecution of their waves consequences of the non-linear system in the upper ionosphere with the assistance of scientific Freja satellite (Holback et al. 1994; De-Jin et al. 1996). Micheal picked a stability in-viscid, in-compressible, and entirely conducting fluid with a parallel uniform motion to their interfaces and also have homologous magnetic fields along the direction of flow (Michael 1955). On the basis of the account of the structure of the linear theory, Michael anticipated that the influence of the magnetic field is stable on a structure. Batiha et al. (2022) developed the solutions of Sturm-Liouville and Langevin equations with fractional operator and proved the existence and uniqueness. Albadarneh et al. (2021) constructed the analytical solutions by utilizing the new proposed scheme poer series method. Shatnawi et al. (2021) investigated the strongly fractional-order nonlinear Benchmark oscillatory problems by using the optimal homotopy asymptotic scheme.

Chandrashekhar has introduced the linear theory for the hegemonize Kelvin-Helmholtz instability in the magnetohydrodynamics of two moving fluids with uniform velocity (Chandrasekhar 1961). Nayfeh inspected the non-linear characteristics of Kelvin-Helmholtz instability concerning an ideal fluid (Hasan and Saric 1971). Kant examined the magnetohydrodynamics with stable wave packets nonlinear progression for the Kelvin-Helmholtz instability (Kant and Malik 1982). Kant proclaimed that the sub-critical magnetohydrodynamics flow with dissimilitude velocity is less than critical velocity. He also investigated that the dynamical model of amplitude generations is fundamentally non-linear Schrödinger equation. Kant also disclosed another point, namely that under the impact of the magnetic field, the magnetic amplitude of waves is unstable for modulation (Kant and Malik 1982). The inverse scattering transformation has been exploited to explore the solution of one-dimensional non-linear Schrödinger and analyzed that the solitary wave solution is expedited by smooth initial information and is also analogous to the final stage of modulation instability (Aleksei and Zakharov 1972).

The analysis of the 4th-order non-linear Schrödinger equation in sort of solitons with Ricatti-Bernoulli sub-ODE and *tanh − coth* expansion method is depicted in Mohamed et al. (2017). Inc investigates the solitonic structures of higher-order dispersive cubic quintic Schrödinger equations Inc et al. (2017). The modified Tanh-Coth scheme and the Riccati-Bernoulli sub-ordinary differential equation have been used to study the solitons of the non-linear evolution equation Inc et al. (2017). Solitary waves of the nonlinear Schrödinger equation have been studied using the fractional operator (Mustafa et al. 2018). The exact solutions of 2 distinct fifth-order non-linear partial differential equations have been

examined using the Riccati-Bernoulli sub-ODE approach (Inc et al. 2017). The dynamic behavior of the ill-posed Boussinesq equation in shallow water and non-linear lattices has explained by Inc Fairouz et al. (2017). In order to study the category of long-wave unstable lubrication models, the Lie theory has been used Adil et al. (2020). Wave propagation in micro-structured solids with conformable time-fractional operators has been illustrated in this study Nauman et al. (2020). The exact Hirota-Maccari travelling wave solutions in the non-linear optics for the $(2 + 1)$-dimensional system (Nauman et al. 2019). The analysis report of the generalised second-order nonlinear Schrödinger equation has been created by Raza Nauman et al. (2020). Asjad investigated 2D-chiral non-linear Schrödinger equation by executing two different techniques Hamood et al. (2021). It has become possible to derive the precise travelling wave solutions to the Schrödinger hyperbolic equation in Hamood-Ur et al. (2020).

The non-linear Schrödinger equations are primitive originators cataloging the physics of optical pulses of light in Kerr non-linearity media. An extensive class of striking and systematized techniques has been reconnoitering canonical and reliable solutions. Some of them are, symmetry strategy George and Kumei (2013), $tanh - coth$ trigonometric function scheme Engui (2000), exp-function technique (Mingliang and Li 2005), Lie and Bäcklund transformation toll (Hai-Ping and Pan 2014) and extended trial equation technique (Nawaz et al. 2017), etc. This article aspires to comparatively analyze extricated traveling wave exact structures of elliptic non-linear schrödinger equation in the perspective of three distinct fractional derivatives and executing new direct extended algebraic strategy. The leading considered model is Seadawy et al. (2020),

$$2i\Psi_t + \Psi_{xx} + \Psi_{yy} = \varrho|\Psi^2|\Psi. \tag{1}$$

This model is describing the phenomenon of the two fluids that were superimposed were separated by the interface at z = 0. The fluids are inviscid, in-compressible, semi-infinite, and conduct perfectly with surface tension at the boundary. The $(2 + 1)$−dimensional dynamical nonlinear elliptic Schrödinger equation provides an illustration of the pulse propagation ahead of ultra-short range in optical communication systems. This model includes optical fibre and optical communication systems as its primary applications.

The current research article is planned as, Sect. 2 is committed for the preliminaries, in Sect. 3 fractional depiction of the governing model, Sect. 4 communicates the anatomization of technique, Sect. 5 reveals the solutions, and terminal Sect. 6 concludes the discussion.

2 Preliminaries

Here, we will dispute some germane notations and contributions which exploit to extract futuristic ideas.

2.1 Conformable fractional operator

Definition 1 Assume that a $h : R^+ \rightarrow R$ is differential function. The conformable derivative with fractional order $0 < \varpi \leq 1$ as Abdeljawad (2015),

$$D_t^\varpi(h(t)) = \lim_{\varepsilon \to 0} \frac{h(t + \varepsilon t^{1-\varpi}) - h(t)}{\varepsilon}, \tag{2}$$

where time is positive.

The fractional derivative's features (Michael 1955).

(**1**) : $D_t^\varpi t^\varsigma = \varsigma t^{\varsigma - \varpi}, \ \forall \varsigma \in R.$

(**2**) : $D_t^\varpi(k(h(t))) = kD_t^\varpi(h(t)).$

(**3**) : $D_t^\varpi(m(h(t)) + n(g(t))) = mD_t^\varpi(h(t)) + nD_t^\varpi(g(t)) \ \forall m, n \in R.$

(**4**) : $D_t^\varpi(\frac{g(t)}{h(t)}) = \frac{(h(t)) \ D_t^\varpi(g(t)) - (g(t)) \ D_t^\varpi(h(t))}{(h(t))^2}.$

(**5**) : $D_t^\varpi(g(t) * h(t)) = (g(t)) \ D_t^\varpi(h(t)) * (h(t)) \ D_t^\varpi(g(t)).$

(**6**) : $D_t^\varpi h(t) = t^{1-\varpi} \frac{dh}{dt}.$

(**7**) : $D_t^\varpi x^\varsigma = \frac{\Gamma(1+\varsigma)}{\Gamma(1+\varsigma-\varpi)} x^{\varsigma - \varpi}, \ \varsigma \geq 0.$

(**8**) : $D_t^\varpi(c) = 0 \ \forall \ constants.$

(**9**) : $D_t^\varpi((h(x) \circ (g(t))) = t^{1-\varpi} g'(t) h'(g(t)).$

2.2 β–fractional derivative

Definition 2 It is defined as Kimeu (2009):,

$$_0^B D_x^\varpi(h(x)) = \lim_{\varepsilon \to 0} \frac{h(x + \varepsilon(x + \frac{1}{\Gamma(\varpi)})) - h(x)}{\varepsilon}, \tag{3}$$

The fractional differential operator's characteristics are Kimeu (2009).

Theorem 1 *Assume* $0 < \varpi < 1$, $m, n, c \in R$ *and differentiable functions* $h(x)$, $g(x)$ *with positive time*:

(**1**) : $_0^B D_x^\varpi(c) = 0, \ \forall \ constants.$

(**2**) : $_0^B D_x^\varpi(\frac{g(x)}{h(x)}) = \frac{(h(x)) \ _0^B D_x^\varpi(g(x)) - (g(x)) \ _0^B D_x^\varpi(h(x))}{(h(x))^2}.$

(**3**) : $_0^B D_x^\varpi(g(x) * h(x)) = (g(x)) \ _0^B D_x^\varpi(h(x)) * (h(x)) \ _0^B D_x^\varpi(g(x)).$

(**4**) : $_0^B D_x^\varpi(m(h(x)) + n(g(x))) = m \ _0^B D_x^\varpi(h(x)) + n \ _0^B D_x^\varpi(g(x)).$

(**5**) : $_0^B D_x^\varpi(k(h(x))) = k \ _0^B D_x^\varpi(g(x))(h(x)).$

2.3 Truncated M-fractional operator

Definition 3 Assume a $h : R^+ \to R$ is differential function, which is define with $0 < \varpi < 1$ fractional order Abdeljawad (2015):

$$_i D_M^{\varpi, \gamma}(h(t)) = \lim_{\varepsilon \to 0} \frac{h(t + {}_i E_\gamma(\varepsilon t^{-\varpi})) - h(t)}{\varepsilon}, \tag{4}$$

where Mittag-leffer function $_iE_\gamma$ with one parameter.

Definition 4 It is defined in Abdeljawad (2015):

$$_iE_\gamma(Z) = \sum_{j=0}^{i} \frac{Z^j}{\Gamma(j\gamma + 1)}, \tag{5}$$

where $Z \in C$ and $\gamma > 0$.

Theorem 2 *As $0 < \varpi \leq 1$, $m, n, c \in R$ and $h(x)$, $g(x)$ are differentiable at $t > o$ so*:

The qualities of a fractional operator include Kimeu (2009):

(**1**) : $_iD_M^{\varpi,\gamma}(m(h(t)) + n(g(t))) = m \ _iD_M^{\varpi,\gamma}(h(t)) + n \ _iD_M^{\varpi,\gamma}(g(t))$.

(**2**) : $_iD_M^{\varpi,\gamma}(g(t) * h(t)) = (g(t)) \ _iD_M^{\varpi,\gamma}(h(t)) * (h(t)) \ _iD_M^{\varpi,\gamma}(g(t))$.

(**3**) : $_iD_M^{\varpi,\gamma}(c) = 0$.

(**4**) : $_iD_M^{\varpi,\gamma}(k(h(t))) = k \ _iD_M^{\varpi,\gamma}(h(t))$.

(**5**) : $_iD_M^{\varpi,\gamma}(t^\vartheta) = T^{\vartheta-\varpi}, \quad \vartheta \in R$.

(**6**) : $_iD_M^{\varpi,\gamma}(h(g))(t) = h'(g \ _iD_M^{\varpi,\gamma}(g))$.

(**7**) : $_iD_M^{\varpi,\gamma}(\frac{g(t)}{h(t)}) = \frac{(h(t)) \ _iD_M^{\varpi,\gamma}(g(t)) - (g(t)) \ _iD_M^{\varpi,\gamma}(h(t))}{(h(t))^2}$.

3 Fractional presentation

The fractional representation of the assumed nonlinear partial differential equation shepherd with three distinct fractional operators.

(**1**): The conformable fractional operator ia applying on Eq. (1),

$$2iD_t^\varpi\Psi + \Psi_{xx} + \Psi_{yy} - \varrho|\Psi|^2\Psi = 0, \tag{6}$$

where D_t^ϖ is the conformable operator concerning to t.

(**2**): The β-operator is applying on Eq. (1),

$$2i \ _0^BD_t^\varpi\Psi + {_0^B}D_{xx}^{2\varpi}\Psi + {_0^B}D_y^{2\varpi}\Psi - \varrho|\Psi|^2\Psi = 0, \tag{7}$$

where $_0^BD_t^\varpi$, $_0^BD_x^\varpi$ and $_0^BD_y^\varpi$ are β-operator with reference to t, x and y respectively.

(**3**): The truncated-M operator is applying on Eq. (1),

$$2i \ _iD_{M,t}^{2\varpi,\gamma}\Psi + {_i}D_{M,x}^{2\varpi,\gamma}\Psi + {_i}D_{M,y}^{2\varpi,\gamma}\Psi - \varrho|\Psi|^2\Psi = 0, \tag{8}$$

where $_iD_{M,t}^{\varpi,\gamma}$, $_iD_{M,x}^{\varpi,\gamma}$ and $_iD_{M,y}^{\varpi,\gamma}$ are the β operators in sense of t, x and y respectively.

3.1 Operational transformations

Here are the re-portable transformations for the anticipated PDE to ODE conversion for the solution of Eqs. (6), (7) and (8).

Let us consider some fractional operator-related functional transformations:

$$\Psi = \Psi(x, y, t), \quad where \quad \Psi(x, y, t) = \Phi(\tau)e^{i\psi}, \tag{9}$$

where Φ is real function and τ and ψ is traced as per concerned fractional operators.

(1): We designate τ and ψ for the conformable fractional operator such as:

$$\tau = \kappa_1 x + \kappa_2 y + (\frac{\sigma}{\varpi})t^{\varpi}, \tag{10}$$

$$\psi = b_1 x + b_2 y + (\frac{\lambda}{\varpi})t^{\varpi} + \theta. \tag{11}$$

(2): We designate τ and ψ for the β fractional operator such as:

$$\tau = \frac{\kappa_1}{\varpi}\left(x + \frac{1}{\Gamma(\varpi)}\right)^{\varpi} + \frac{\kappa_2}{\varpi}\left(y + \frac{1}{\Gamma(\varpi)}\right)^{\varpi} + \frac{\sigma}{\varpi}\left(t + \frac{1}{\Gamma(\varpi)}\right)^{\varpi}, \tag{12}$$

$$\psi = \frac{b_1}{\varpi}\left(x + \frac{1}{\Gamma(\varpi)}\right)^{\varpi} + \frac{b_2}{\varpi}\left(y + \frac{1}{\Gamma(\varpi)}\right)^{\varpi} + \frac{\lambda}{\varpi}\left(t + \frac{1}{\Gamma(\varpi)}\right)^{\varpi} + \theta_0(\tau). \tag{13}$$

(3): We designate τ and ψ for the truncated M-fractional operator such as:

$$\tau = \frac{\Gamma(\gamma + 1)}{\varpi}(\kappa_1 x^{\varpi} + \kappa_2 y^{\varpi} + \sigma t^{\varpi}), \tag{14}$$

$$\psi = \frac{\Gamma(\gamma + 1)}{\varpi}(b_1 x^{\varpi} + b_2 y^{\varpi} + \lambda t^{\varpi}) + \theta_0(\tau), \tag{15}$$

where $\Phi(\tau)$ is the real function, ψ interprets the phase factor, frequency is reported by λ, b_1 and b_2 are wave number.

4 New extended direct algebraic method

The proposed scheme is following Ali et al. (2020).

Assume a general non-linear partial differential equation:

$$P(\Psi, \Psi_t, \Psi_x, \Psi_y, \Psi_{tt}, \Psi_{xx}, ...) = 0. \tag{16}$$

It has susceptibility to attain the form of non-linear ordinary differential equation on the execution of complex traveling wave transformation such as:

$$\Psi(x, y, t) = \Phi(\tau)e^{i\psi}, \tag{17}$$

where $\tau = \kappa_1 t + \kappa_2 x + \kappa_3 y$ and $\psi = \kappa_4 t + \kappa_5 x + \kappa_6 y + \theta$, we get:

$$F(\Phi, \Phi', \Phi'', ...) = 0, \tag{18}$$

here, the notation of differentiation depicted by the prime in Eq. (18).

Assume that solution of Eq. (18) is:

$$F(\tau) = a_0 + \sum_{i=-m}^{m} \left[a_i (P(\tau))^i \right], \tag{19}$$

where,

$$P'(\tau) = \ln(\rho) \left(\mu_2 + v_2 P(\tau) + \zeta_2 P^2(\tau) \right), \quad \rho \neq 0, 1, \tag{20}$$

where ζ_2, μ_2 and v_2 are real constants.

The general solutions with respect to parameters μ_2, v_2 and ζ_2 of Eq. (20) are:

(Case 1): When $v_2^2 - 4\mu_2\zeta_2 < 0$ and $\zeta_2 \neq 0$,

$$P_1(\tau) = -\frac{v_2}{2\zeta_2} + \frac{\sqrt{-\Theta}}{2\zeta_2} \tan_\rho \left(\frac{\sqrt{-\Theta}}{2} \tau \right). \tag{21}$$

$$P_2(\tau) = -\frac{v_2}{2\zeta_2} - \frac{\sqrt{-\Theta}}{2\zeta_2} \cot_\rho \left(\frac{\sqrt{-\Theta}}{2} \tau \right). \tag{22}$$

$$P_3(\tau) = -\frac{v_2}{2\zeta_2} + \frac{\sqrt{-\Theta}}{2\zeta_2} \left(\tan_\rho \left(\sqrt{-\Theta}\tau \right) \pm \sqrt{mn} \sec_\rho \left(\sqrt{-\Theta}\tau \right) \right). \tag{23}$$

$$P_4(\tau) = -\frac{v_2}{2\zeta_2} + \frac{\sqrt{-\Theta}}{2\zeta_2} \left(\cot_\rho \left(\sqrt{-\Theta}\tau \right) \pm \sqrt{mn} \csc_\rho \left(\sqrt{-\Theta}\tau \right) \right). \tag{24}$$

$$P_5(\tau) = -\frac{v_2}{2\zeta_2} + \frac{\sqrt{-\Theta}}{4\zeta_2} \left(\tan_\rho \left(\frac{\sqrt{-\Theta}}{4} \tau \right) - \cot_\rho \left(\frac{\sqrt{-\Theta}}{4} \tau \right) \right). \tag{25}$$

(Case 2): When $v_2^2 - 4\mu_2\zeta_2 > 0$ and $\zeta_2 \neq 0$,

$$P_6(\tau) = -\frac{v_2}{2\zeta_2} - \frac{\sqrt{\Theta}}{2\zeta_2} \tanh_\rho \left(\frac{\sqrt{\Theta}}{2} \tau \right). \tag{26}$$

$$P_7(\tau) = -\frac{v_2}{2\zeta_2} - \frac{\sqrt{\Theta}}{2\zeta_2} \coth_\rho \left(\frac{\sqrt{\Theta}}{2} \tau \right). \tag{27}$$

$$P_8(\tau) = -\frac{v_2}{2\zeta_2} + \frac{\sqrt{\Theta}}{2\zeta_2} \left(-\tanh_\rho \left(\sqrt{\Theta}\tau \right) \pm i\sqrt{mn} \, sech_\rho \left(\sqrt{\Theta}\tau \right) \right). \tag{28}$$

$$P_9(\tau) = -\frac{v_2}{2\zeta_2} + \frac{\sqrt{\Theta}}{2\zeta_2}\left(-\coth_\rho\left(\sqrt{\Theta}\tau\right) \pm \sqrt{mn}\,\mathrm{csch}_\rho\left(\sqrt{\Theta}\tau\right)\right). \tag{29}$$

$$P_{10}(\tau) = -\frac{v_2}{2\zeta_2} - \frac{\sqrt{\Theta}}{4\zeta_2}\left(\tanh_\rho\left(\frac{\sqrt{\Theta}}{4}\tau\right) + \coth_\rho\left(\frac{\sqrt{\Theta}}{4}\tau\right)\right). \tag{30}$$

(Case 3): When $\mu_2\zeta_2 > 0$ and $v_2 = 0$,

$$P_{11}(\tau) = \sqrt{\frac{\mu_2}{\zeta_2}}\,\tan_\rho\left(\sqrt{\mu_2\zeta_2}\,\tau\right). \tag{31}$$

$$P_{12}(\tau) = -\sqrt{\frac{\mu_2}{\zeta_2}}\,\cot_\rho\left(\sqrt{\mu_2\zeta_2}\,\tau\right). \tag{32}$$

$$P_{13}(\tau) = \sqrt{\frac{\mu_2}{\zeta_2}}\left(\tan_\rho\left(2\sqrt{\mu_2\zeta_2}\,\tau\right) \pm \sqrt{mn}\,\sec_\rho\left(2\sqrt{\mu_2\zeta_2}\,\tau\right)\right). \tag{33}$$

$$P_{14}(\tau) = \sqrt{\frac{\mu_2}{\zeta_2}}\left(-\cot_\rho\left(2\sqrt{\mu_2\zeta_2}\,\tau\right) \pm \sqrt{mn}\,\mathrm{csc}_\rho\left(2\sqrt{\mu_2\zeta_2}\,\tau\right)\right). \tag{34}$$

$$P_{15}(\tau) = \frac{1}{2}\sqrt{\frac{\mu_2}{\zeta_2}}\left(\tan_\rho\left(\frac{\sqrt{\mu_2\zeta_2}}{2}\tau\right) - \cot_\rho\left(\frac{\sqrt{\mu_2\zeta_2}}{2}\tau\right)\right). \tag{35}$$

(Case 4): When $\mu_2\zeta_2 < 0$ and $v_2 = 0$,

$$P_{16}(\tau) = -\sqrt{-\frac{\mu_2}{\zeta_2}}\,\tanh_\rho\left(\sqrt{-\mu_2\zeta_2}\,\tau\right). \tag{36}$$

$$P_{17}(\tau) = -\sqrt{-\frac{\mu_2}{\zeta_2}}\,\coth_\rho\left(\sqrt{-\mu_2\zeta_2}\,\tau\right). \tag{37}$$

$$P_{18}(\tau) = \sqrt{-\frac{\mu_2}{\zeta_2}}\left(-\tanh_\rho\left(2\sqrt{-\mu_2\zeta_2}\,\tau\right) \pm i\sqrt{mn}\,\mathrm{sech}_\rho\left(2\sqrt{-\mu_2\zeta_2}\,\tau\right)\right). \tag{38}$$

$$P_{19}(\tau) = \sqrt{-\frac{\mu_2}{\zeta_2}}\left(-\coth_\rho\left(2\sqrt{-\mu_2\zeta_2}\,\tau\right) \pm \sqrt{mn}\,\mathrm{csch}_\rho\left(2\sqrt{-\mu_2\zeta_2}\,\tau\right)\right). \tag{39}$$

$$P_{20}(\tau) = -\frac{1}{2}\sqrt{-\frac{\mu_2}{\zeta_2}}\left(\tanh_\rho\left(\frac{\sqrt{-\mu_2\zeta_2}}{2}\tau\right) + \coth_\rho\left(\frac{\sqrt{-\mu_2\zeta_2}}{2}\tau\right)\right). \tag{40}$$

(Case 5): When $v_2 = 0$ and $\mu_2 = \zeta_2$,

$$P_{21}(\tau) = \tan_\rho \left(\mu_2 \tau \right). \tag{41}$$

$$P_{22}(\tau) = - \cot_\rho \left(\mu_2 \tau \right). \tag{42}$$

$$P_{23}(\tau) = \tan_\rho \left(2\mu_2 \tau \right) \pm \sqrt{mn} \sec_\rho \left(2\mu_2 \tau \right). \tag{43}$$

$$P_{24}(\tau) = - \cot_\rho \left(2\mu_2 \tau \right) \pm \sqrt{mn} \csc_\rho \left(2\mu_2 \tau \right). \tag{44}$$

$$P_{25}(\tau) = \frac{1}{2} \left(\tan_\rho \left(\frac{\mu_2}{2} \tau \right) - \cot_\rho \left(\frac{\mu_2}{2} \tau \right) \right). \tag{45}$$

(Case 6): When $\nu_2 = 0$ and $\zeta_2 = -\mu_2$,

$$P_{26}(\tau) = - \tanh_\rho \left(\mu_2 \tau \right). \tag{46}$$

$$P_{27}(\tau) = - \coth_\rho \left(\mu_2 \tau \right). \tag{47}$$

$$P_{28}(\tau) = - \tanh_\rho \left(2\mu_2 \tau \right) \pm i\sqrt{mn} \, sech_\rho \left(2\mu_2 \tau \right). \tag{48}$$

$$P_{29}(\tau) = - \cot_\rho \left(2\mu_2 \tau \right) \pm \sqrt{mn} \, csch_\rho \left(2\mu_2 \tau \right). \tag{49}$$

$$P_{30}(\tau) = - \frac{1}{2} \left(\tanh_\rho \left(\frac{\mu_2}{2} \tau \right) + \cot_\rho \left(\frac{\mu_2}{2} \tau \right) \right). \tag{50}$$

(Case 7): When $\nu_2^2 = 4\mu_2 \zeta_2$,

$$P_{31}(\tau) = \frac{-2\mu_2 (\nu_2 \tau \ln \rho + 2)}{\nu_2^2 \tau \ln \rho}. \tag{51}$$

(Case 8): When $\nu_2 = p, \mu_2 = pq, (q \neq 0)$ and $\zeta_2 = 0$,

$$P_{32}(\tau) = \rho^{p\tau} - q. \tag{52}$$

(Case 9): When $\nu_2 = \zeta_2 = 0$,

$$P_{33}(\tau) = \mu_2 \tau \ln \rho. \tag{53}$$

(Case 10): When $\nu_2 = \mu_2 = 0$,

$$P_{34}(\tau) = \frac{-1}{\zeta_2 \tau \ln \rho}. \tag{54}$$

(Case 11): When $\mu_2 = 0$ and $\nu_2 \neq 0$,

$$P_{35}(\tau) = - \frac{m\nu_2}{\zeta_2 \left(\cosh_\rho \left(\nu_2 \tau \right) - \sinh_\rho \left(\nu_2 \tau \right) + m \right)}. \tag{55}$$

$$P_{36}(\tau) = -\frac{v_2\left(\sinh_\rho\left(v_2\tau\right) + \cosh_\rho\left(v_2\tau\right)\right)}{\zeta_2\left(\sinh_\rho\left(v_2\tau\right) + \cosh_\rho\left(v_2\tau\right) + n\right)}. \tag{56}$$

(Case 12): When $v_2 = p, \zeta_2 = pq, \ (q \neq 0 \text{ and } \mu_2 = 0)$,

$$P_{37}(\tau) = -\frac{m\rho^{p\tau}}{m - qn\rho^{p\tau}}.$$

$$\sinh_\rho(\tau) = \frac{m\rho^\tau - n\rho^{-\tau}}{2}, \quad \cosh_\rho(\tau) = \frac{m\rho^\tau + n\rho^{-\tau}}{2},$$

$$\tanh_\rho(\tau) = \frac{m\rho^\tau - n\rho^{-\tau}}{m\rho^\tau + n\rho^{-\tau}}, \quad \coth_\rho(\tau) = \frac{m\rho^\tau + n\rho^{-\tau}}{m\rho^\tau - n\rho^{-\tau}},$$

$$sech_\rho(\tau) = \frac{2}{m\rho^\tau + n\rho^{-\tau}}, \quad csch_\rho(\tau) = \frac{2}{m\rho^\tau - n\rho^{-\tau}}, \tag{57}$$

$$\sin_\rho(\tau) = \frac{m\rho^{i\tau} - n\rho^{-i\tau}}{2i}, \quad coP_\rho(\tau) = \frac{m\rho^{i\tau} + n\rho^{-i\tau}}{2},$$

$$\tan_\rho(\tau) = -i\frac{m\rho^{i\tau} - n\rho^{-i\tau}}{m\rho^{i\tau} + n\rho^{-i\tau}}, \quad \cot_\rho(\tau) = i\frac{m\rho^{i\tau} + n\rho^{-i\tau}}{m\rho^{i\tau} - n\rho^{-i\tau}},$$

$$\sec_\rho(\tau) = \frac{2}{m\rho^\tau + n\rho^{-\tau}}, \quad \csc_\rho(\tau) = \frac{2i}{m\rho^\tau - n\rho^{-\tau}},$$

The deformation parameters m and n are arbitrary constants greater than zero.

4.1 Application to Eq. (16)

Operating the Eq. (9) to the Eqs. (6), (7) and (8) and equating real and imaginary part respectively:

$$(\kappa_1^2 + \kappa_2^2)\Phi'' - (b_1^2 + b_2^2 + 2\lambda)\Phi - \varrho\Phi^3 = 0. \tag{58}$$

$$\sigma = -\kappa_1 b_1 - \kappa_2 b_2. \tag{59}$$

Plugging the homogeneous balancing constant in Eq. (19), thus the solution is:

$$\Phi(\tau) = a_0 + a_1(P(\tau)), \tag{60}$$

where,

$$P'(\tau) = \ln(\rho)\left(\mu_2 + v_2 P(\tau) + \zeta_2 P^2(\tau)\right), \quad \rho \neq 0, 1. \tag{61}$$

The predicted solution Eq. (60) subsituting in Eq. (58) and separating the coefficient of different powers of (τ), thus we have an algebraic system of equations.

The acquired algebraic system solve with the assistance of `Mathematica` and obtain:

$$\left[a_0 = \pm \frac{v_2 \sqrt{\kappa_1^2 + \kappa_2^2} \log[\rho]}{\sqrt{2\varrho}}, \ a_1 = \pm \frac{2\zeta_2 \sqrt{\kappa_1^2 + \kappa_2^2} \log[\rho]}{\sqrt{2\varrho}}, \right.$$

$$\left. \lambda = -\frac{b_1^2 + b_2^2}{2} - \frac{(\kappa_1^2 + \kappa_2^2)\Theta \log[\rho]^2}{4}, \right] \tag{62}$$

where,

$$\Theta = v_2^2 - 4\mu_2\zeta_2.$$

The general solution of Eq. (1) by plugging Eq. (62) in Eq. (19) is:

$$\Psi(x, y, t) = \pm \frac{v_2 \sqrt{\kappa_1^2 + \kappa_2^2} \log[\rho]}{\sqrt{2\varrho}} \pm \frac{2\zeta_2 \sqrt{\kappa_1^2 + \kappa_2^2} \log[\rho]}{\sqrt{2\varrho}} \left(P_i(\tau) \right). \tag{63}$$

5 Traveling wave solution

Now, we will acquire distinct solutions by choosing P_i from (21)–(57) respectively.

(Case 1): When $v_2^2 - 4\mu_2\zeta_2 < 0$ and $\zeta_2 \neq 0$,

$$\Psi_1(x, y, t) = \pm \Upsilon \sqrt{-\Theta} \tan_\rho \left(\frac{\sqrt{-\Theta}}{2} \tau \right). \tag{64}$$

$$\Psi_2(x, y, t) = \mp \Upsilon \sqrt{-\Theta} \cot_\rho \left(\frac{\sqrt{-\Theta}}{2} \tau \right). \tag{65}$$

$$\Psi_3(x, y, t) = \pm \Upsilon \sqrt{-\Theta} \left(\tan_\rho \left(\sqrt{-\Theta}\tau \right) \pm \sqrt{mn} \sec_\rho \left(\sqrt{-\Theta}\tau \right) \right). \tag{66}$$

$$\Psi_4(x, y, t) = \pm \Upsilon \sqrt{-\Theta} \left(\cot_\rho \left(\sqrt{-\Theta}\tau \right) \pm \sqrt{mn} \csc_\rho \left(\sqrt{-\Theta}\tau \right) \right). \tag{67}$$

$$\Psi_5(x, y, t) = \pm \Upsilon \sqrt{-\Theta} \left(\tan_\rho \left(\frac{\sqrt{-\Theta}}{4} \tau \right) - \cot_\rho \left(\frac{\sqrt{-\Theta}}{4} \tau \right) \right). \tag{68}$$

(Case 2): When $v_2^2 - 4\mu_2\zeta_2 > 0$ and $\zeta_2 \neq 0$,

$$\Psi_6(x, y, t) = \mp \Upsilon \sqrt{-\Theta} \tanh_\rho \left(\frac{\sqrt{\Theta}}{2} \tau \right). \tag{69}$$

$$\Psi_7(\tau) = \mp \Upsilon \sqrt{-\Theta} \coth_\rho \left(\frac{\sqrt{\Theta}}{2} \tau \right). \tag{70}$$

$$\Psi_8(x, y, t) = \pm \Upsilon \sqrt{-\Theta} \left(-\tanh_\rho \left(\sqrt{\Theta} \tau \right) \pm i\sqrt{mn} \mathrm{sech}_\rho \left(\sqrt{\Theta} \tau \right) \right). \tag{71}$$

$$\Psi_9(x, y, t) = \pm \Upsilon \sqrt{-\Theta} \left(-\coth_\rho \left(\sqrt{\Theta} \tau \right) \pm \sqrt{mn} \mathrm{csch}_\rho \left(\sqrt{\Theta} \tau \right) \right). \tag{72}$$

$$\Psi_{10}(x, y, t) = \mp \Upsilon \sqrt{-\Theta} 4\zeta_2 \left(\tanh_\rho \left(\frac{\sqrt{\Theta}}{4} \tau \right) + \coth_\rho \left(\frac{\sqrt{\Theta}}{4} \tau \right) \right). \tag{73}$$

(Case 3): When $\mu_2\zeta_2 > 0$ and $\nu_2 = 0$,

$$\Psi_{11}(x, y, t) = \pm 2\Upsilon \left(\sqrt{\zeta_2\mu_2} \tan_\rho \left(\sqrt{\mu_2\zeta_2} \tau \right) \right). \tag{74}$$

$$\Psi_{12}(x, y, t) = \mp 2\Upsilon \left(\sqrt{\zeta_2\mu_2} \cot_\rho \left(\sqrt{\mu_2\zeta_2} \tau \right) \right). \tag{75}$$

$$\Psi_{13}(x, y, t) = \pm 2\Upsilon \sqrt{\zeta_2\mu_2} \left(\tan_\rho \left(2\sqrt{\mu_2\zeta_2} \tau \right) \pm \sqrt{mn} \sec_\rho \left(2\sqrt{\mu_2\zeta_2} \tau \right) \right). \tag{76}$$

$$\Psi_{14}(x, y, t) = \pm 2\Upsilon \sqrt{\zeta_2\mu_2} \left(-\cot_\rho \left(2\sqrt{\mu_2\zeta_2} \tau \right) \pm \sqrt{mn} \csc_\rho \left(2\sqrt{\mu_2\zeta_2} \tau \right) \right). \tag{77}$$

$$\Psi_{15}(x, y, t) = \pm \Upsilon \sqrt{\zeta_2\mu_2} \left(\tan_\rho \left(\frac{\sqrt{\mu_2\zeta_2}}{2} \tau \right) - \cot_\rho \left(\frac{\sqrt{\mu_2\zeta_2}}{2} \tau \right) \right). \tag{78}$$

(Case 4): When $\mu_2\zeta_2 < 0$ and $\nu_2 = 0$,

$$\Psi_{16}(x, y, t) = \mp 2\Upsilon \sqrt{-\mu_2\zeta_2} \tanh_\rho \left(\sqrt{-\mu_2\zeta_2} \tau \right). \tag{79}$$

$$\Psi_{17}(x, y, t) = \mp 2\Upsilon \sqrt{-\mu_2\zeta_2} \coth_\rho \left(\sqrt{-\mu_2\zeta_2} \tau \right). \tag{80}$$

$$\Psi_{18}(x, y, t) = \pm 2\Upsilon \sqrt{-\mu_2\zeta_2} \left(-\tanh_\rho \left(2\sqrt{-\mu_2\zeta_2} \tau \right) \pm i\sqrt{mn} \mathrm{sech}_\rho \left(2\sqrt{-\mu_2\zeta_2} \tau \right) \right). \tag{81}$$

$$\Psi_{19}(x, y, t) = \pm 2\Upsilon \sqrt{-\mu_2\zeta_2} \left(-\coth_\rho \left(2\sqrt{-\mu_2\zeta_2} \tau \right) \pm \sqrt{mn} \, csch_\rho \left(2\sqrt{-\mu_2\zeta_2} \tau \right) \right). \tag{82}$$

$$\Psi_{20}(x, y, t) = \mp \Upsilon \sqrt{-\mu_2\zeta_2} \left(\tanh_\rho \left(\frac{\sqrt{-\mu_2\zeta_2}}{2} \tau \right) + \coth_\rho \left(\frac{\sqrt{-\mu_2\zeta_2}}{2} \tau \right) \right). \tag{83}$$

(Case 5): When $\nu_2 = 0$ and $\mu_2 = \zeta_2$,

$$\Psi_{21}(x, y, t) = \pm 2\zeta_2 \Upsilon \big(\tan_\rho \big(\zeta_2 \tau \big) \big). \tag{84}$$

$$\Psi_{22}(x, y, t) = \mp 2\zeta_2 \Upsilon \big(\cot_\rho \big(\zeta_2 \tau \big) \big). \tag{85}$$

$$\Psi_{23}(x, y, t) = \pm 2\zeta_2 \Upsilon \Big(\tan_\rho \big(2\zeta_2 \tau \big) \pm \sqrt{mn} \sec_\rho \big(2\zeta_2 \tau \big) \Big). \tag{86}$$

$$\Psi_{24}(x, y, t) = \pm 2\zeta_2 \Upsilon \Big(-\cot_\rho \big(2\zeta_2 \tau \big) \pm \sqrt{mn} \csc_\rho \big(2\zeta_2 \tau \big) \Big). \tag{87}$$

$$\Psi_{25}(x, y, t) = \pm \zeta_2 \Upsilon \left(\tan_\rho \left(\frac{\zeta_2}{2} \tau \right) - \cot_\rho \left(\frac{\zeta_2}{2} \tau \right) \right). \tag{88}$$

(Case 6): When $v_2 = 0$ and $\zeta_2 = -\mu_2$,

$$\Psi_{26}(x, y, t) = \pm 2\mu_2 \Upsilon \tanh_\rho \big(\mu_2 \tau \big). \tag{89}$$

$$\Psi_{27}(x, y, t) = \pm 2\mu_2 \Upsilon \coth_\rho \big(\mu_2 \tau \big). \tag{90}$$

$$\Psi_{28}(x, y, t) = \mp 2\mu_2 \Upsilon \Big(-\tanh_\rho \big(2\mu_2 \tau \big) \pm i\sqrt{mn} \, sech_\rho \big(2\mu_2 \tau \big) \Big). \tag{91}$$

$$\Psi_{29}(x, y, t) = \mp 2\mu_2 \Upsilon \Big(-\cot_\rho \big(2\mu_2 \tau \big) \pm \sqrt{mn} \, csch_\rho \big(2\mu_2 \tau \big) \Big). \tag{92}$$

$$\Psi_{30}(x, y, t) = \pm \mu_2 \Upsilon \left(\tanh_\rho \left(\frac{\mu_2}{2} \tau \right) + \cot_\rho \left(\frac{\mu_2}{2} \tau \right) \right). \tag{93}$$

(Case 7): When $v_2^2 = 4\mu_2 \zeta_2$,

$$\Psi_{31}(x, y, t) = \pm v_2 \Upsilon \mp 4\zeta_2 \Upsilon \left(\frac{\mu_2 (v_2 \tau \ln \rho + 2)}{v_2^2 \tau \ln \rho} \right). \tag{94}$$

(Case 8): When $v_2 = p, \mu_2 = pq, (q \neq 0)$ and $\zeta_2 = 0$,

$$\Psi_{32}(x, y, t) = trivial. \tag{95}$$

(Case 9): When $v_2 = \zeta_2 = 0$,

$$\Psi_{33}(x, y, t) = 0. \tag{96}$$

(Case 10): When $v_2 = \mu_2 = 0$,

$$\Psi_{34}(x, y, t) = \mp 2\Upsilon \left(\frac{1}{\tau \ln \rho} \right). \tag{97}$$

(Case 11): When $\mu_2 = 0$ and $v_2 \neq 0$,

$$\Psi_{35}(x, y, t) = \pm \, \nu_2 \Upsilon \mp 2\Upsilon \left(\frac{m\nu_2}{\left(\cosh_\rho \left(\nu_2 \tau\right) - \sinh_\rho \left(\nu_2 \tau\right) + m\right)} \right). \tag{98}$$

$$\Psi_{36}(x, y, t) = \pm \, \nu_2 \Upsilon \mp 2\Upsilon \left(\frac{\nu_2 \left(\sinh_\rho \left(\nu_2 \tau\right) + \cosh_\rho \left(\nu_2 \tau\right)\right)}{\left(\sinh_\rho \left(\nu_2 \tau\right) + \cosh_\rho \left(\nu_2 \tau\right) + n\right)} \right). \tag{99}$$

(Case 12): When $\nu_2 = p, \zeta_2 = pq, \ (q \neq 0$ and $\mu_2 = 0)$,

$$\Psi_{37}(x, y, t) = \pm p\Upsilon \mp 2pq\Upsilon \left(\frac{m\rho^{p\tau}}{m - qn\rho^{p\tau}} \right), \tag{100}$$

where,

$$\Upsilon = \pm \frac{\sqrt{\kappa_1^2 + \kappa_2^2} \, \log[\rho]}{\sqrt{2\varrho}}.$$

The parameters τ and ψ are set out as Eqs. (10, 11), Eqs. (12, 13) and Eqs. (14, 15) associated with conformable operator, β-operator and truncated M-fractional operator respectively.

6 Graphically review

The fractional order of the operators is belonging to (0,1). There are infinite non-integer values in (0,1), so one can choose the value fractional order according to physical phenomenon. In this study we need to investigate the model and compare the results, thus choose the different values of fractional order from interval with sub-diffusivity.

Figure 1: Depicts the 3D graphic comparison of dissimilar fractional differential operators for Ψ_{21} at the variation of fractional order along with practicable parametric values such as, $\rho = e, \ \kappa_1 = 1, \ \kappa_2 = 1, \ b_1 = 1, \ b_2 = 1, \ \zeta_2 = 1$ and $\varrho = 1$.

Figure 1a–c yields 3D illustration at $\varpi = 0.1$ concerning to conformable operator, $\beta-$ fractional definition and truncated M-fractional derivative respectively.

Figure 1d–f yields 3D illustration at $\varpi = 0.5$ concerning to conformable operator, $\beta-$ fractional definition and truncated M-fractional derivative respectively.

On the account of analysis, the β and truncated M-fractional definitions rendering almost symmetrical curve with little bit difference, however, conformable fractional derivative interprets a prominent variance rather than β and truncated M-fractional operator.
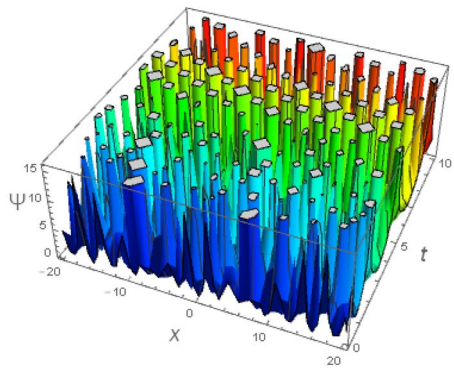
Figure 2: Chronicle the 3D and 2D graphic comparison of dissimilar fractional differential operators for Ψ_{21} at the variation of fractional order along with practicable parametric values such as, $\rho = e, \ \kappa_1 = 1, \ \kappa_2 = 1, \ b_1 = 1, \ b_2 = 1, \ \zeta_2 = 1$ *and* $\varrho = 1$.

Figure 2a–c yields 3D illustration at $\varpi = 0.9$ concerning to conformable operator, $\beta-$ fractional definition and truncated M-fractional derivative respectively.

On the account of 3D analysis, the β and truncated M-fractional definitions rendering almost symmetrical curve with little bit difference, however, conformable fractional derivative interprets a prominent variance rather than β and truncated M-fractional operator.
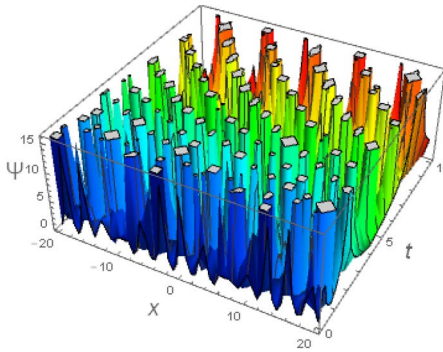
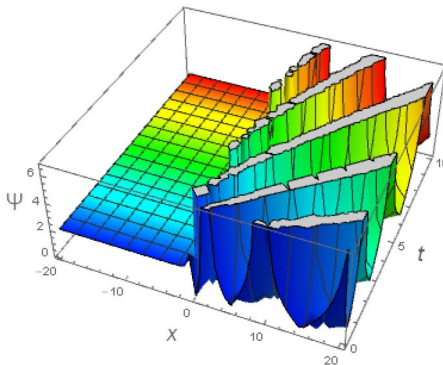(a) 3D delineation for conformable operator at $\varpi = 0.1$.
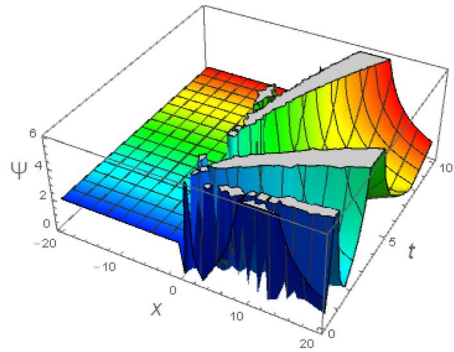
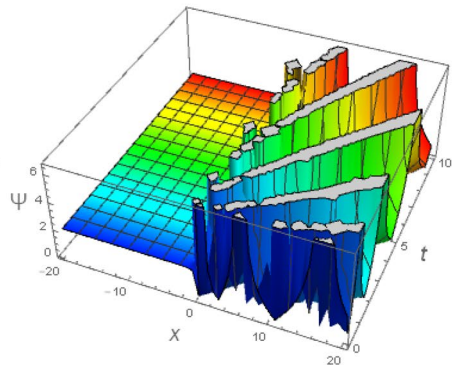(b) 3D delineation for β-operator at $\varpi = 0.1$.
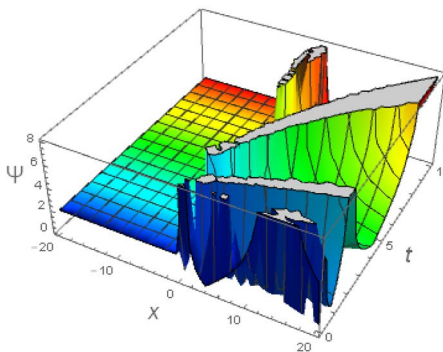
(c) 3D delineation for M-truncated operator at $\varpi = 0.1$.

(d) 3D delineation for conformable operator at $\varpi = 0.5$.

(e) 3D delineation for β-operator at $\varpi = 0.5$.

(f) 3D delineation for M-truncated operator at $\varpi = 0.5$.

Fig. 1 3D portraying for Ψ_{21} with the disparity of fractional operators and fractional order

Figure 2d capitulate 2D comparision of utilized fractional definitions at $\varpi = 0.1$, Fig. 2e remit 2D comparision of executed fractional definitions at $\varpi = 0.3$, and Fig. 2f permit 2D comparision of exploited fractional definitions at $\varpi = 0.5$.
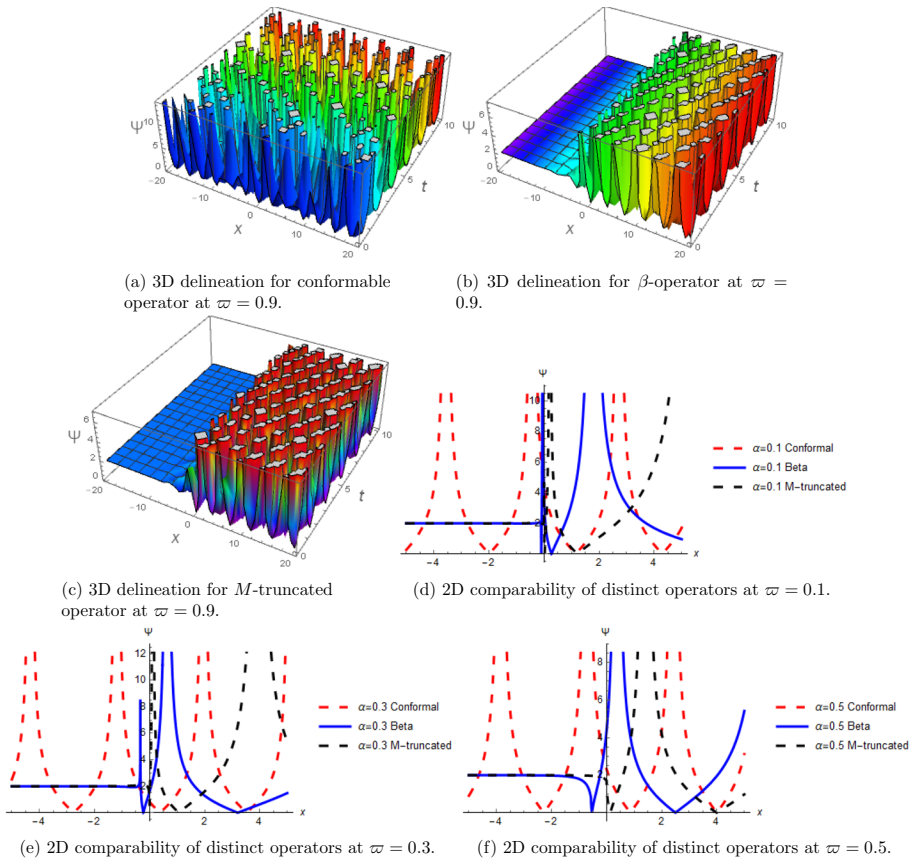
(a) 3D delineation for conformable operator at $\varpi = 0.9$.

(b) 3D delineation for β-operator at $\varpi = 0.9$.

(c) 3D delineation for M-truncated operator at $\varpi = 0.9$.

(d) 2D comparability of distinct operators at $\varpi = 0.1$.

(e) 2D comparability of distinct operators at $\varpi = 0.3$.

(f) 2D comparability of distinct operators at $\varpi = 0.5$.

Fig. 2 2D and 3D portraying for Ψ_{21} with the disparity of fractional operators and fractional order

On the whole 2D inspection, the β and truncated M-fractional definitions manifesting almost the same pattern with little bit difference, however, conformable fractional derivative interprets a prominent variance rather than β and truncated M-fractional operator.

Figure 3 Represent the 2D graphic comparison of dissimilar fractional differential operators for Ψ_{21} at the variation of fractional order along with practicable parametric values such as, $\rho = e$, $\kappa_1 = 1$, $\kappa_2 = 1$, $b_1 = 1$, $b_2 = 1$, $\zeta_2 = 1$ and $\varrho = 1$.

Figure 3a capitulate 2D comparision of utilized fractional definitions at $\varpi = 0.1$, Fig. 3b remit 2D comparision of executed fractional definitions at $\varpi = 0.3$ and display the same locus as described above for 2D in Fig. 2.

Figure 3c contribute 2D comparision for conformable operator by varying fractional order, Fig. 3d contribute 2D comparision for β operator by varying fractional order, and Fig. 3e contribute 2D comparision for truncated M-fractional operator by varying fractional order.

Figure 3f delineates the comparison of prosecuted operators at classical order of derivative, which presents the efficiency of operators.
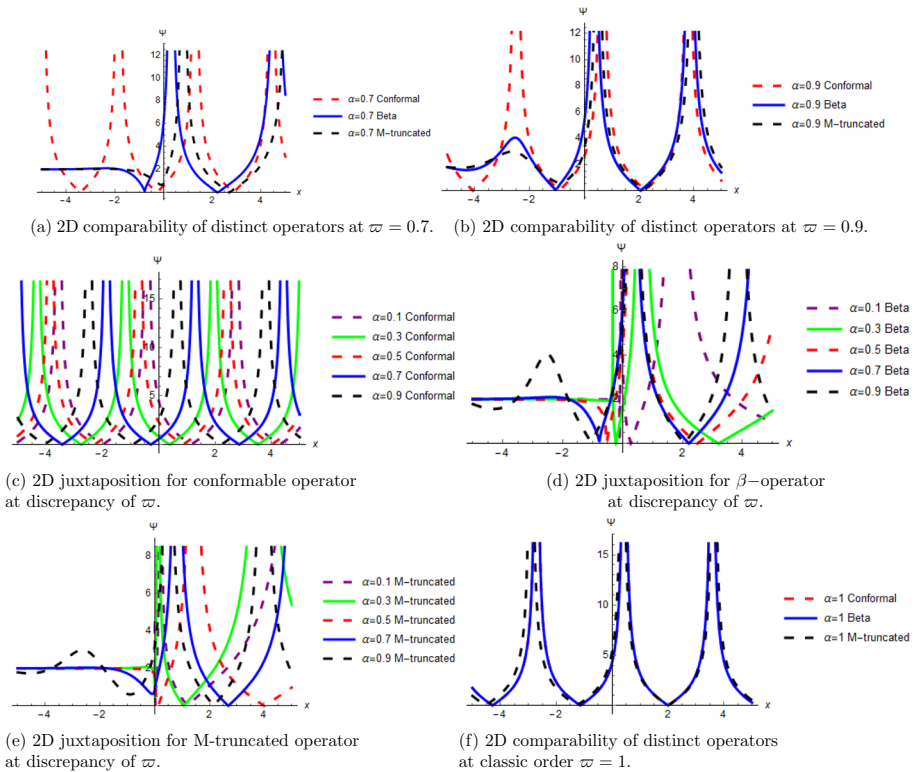
(a) 2D comparability of distinct operators at $\varpi = 0.7$.

(b) 2D comparability of distinct operators at $\varpi = 0.9$.

(c) 2D juxtaposition for conformable operator at discrepancy of ϖ.

(d) 2D juxtaposition for $\beta-$operator at discrepancy of ϖ.

(e) 2D juxtaposition for M-truncated operator at discrepancy of ϖ.

(f) 2D comparability of distinct operators at classic order $\varpi = 1$.

Fig. 3 2D portraying for Ψ_{21} with the disparity of fractional operators and fractional order and also comparision at classic order

Entirely, when we analyzed all fractional 2D presentations against a single solution from the perspective of classical 2D presentation, thus we concluded that fractional study interprets deep knowledge of natural phenomenon rather than classical theory.

Remark The solution Ψ_{21} is displaying the periodic-singular and dark-periodic- singular soliton solution as the fractional order increasing towards classical order.

Figure 4: Depicts the 3D graphic comparison of dissimilar fractional differential operators for Ψ_{36} at the variation of fractional order along with practicable parametric values such as, $\rho = e$, $\kappa_1 = 1$, $\kappa_2 = 1$, $b_1 = 1$, $b_2 = 1$, $v_2 = 1$ *and* $\varrho = 1$.

Figure 4a–c yields 3D illustration at $\varpi = 0.1$ concerning to conformable operator, $\beta-$fractional definition and truncated M-fractional derivative respectively.

Figure 4d–f yields 3D illustration at $\varpi = 0.5$ concerning to conformable operator, $\beta-$fractional definition and truncated M-fractional derivative respectively.

On the account of analysis, the conformable and truncated M-fractional definitions rendering almost symmetrical curve with little bit difference, however, β fractional derivative interprets a prominent variance rather than β and truncated M-fractional operator.
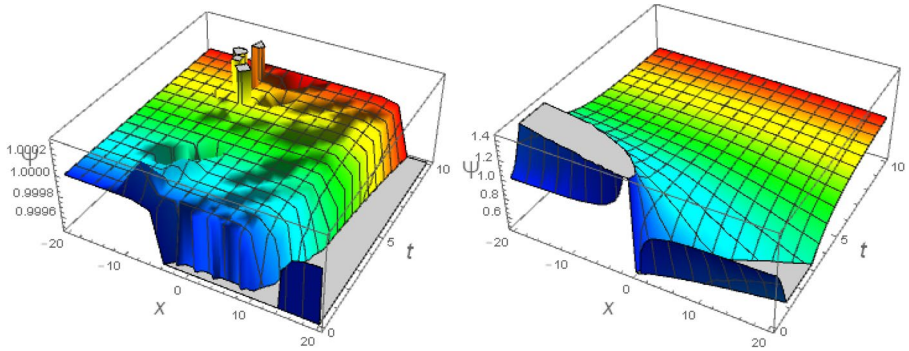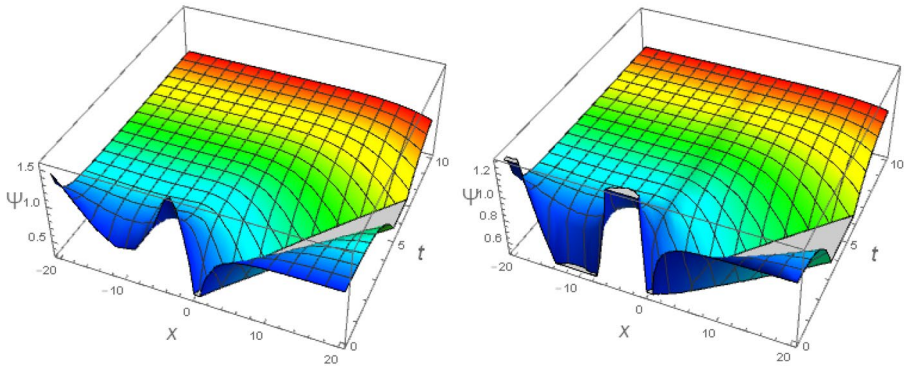
(a) 3D delineation for conformable operator at $\varpi = 0.1$.

(b) 3D delineation for β-operator at $\varpi = 0.1$.
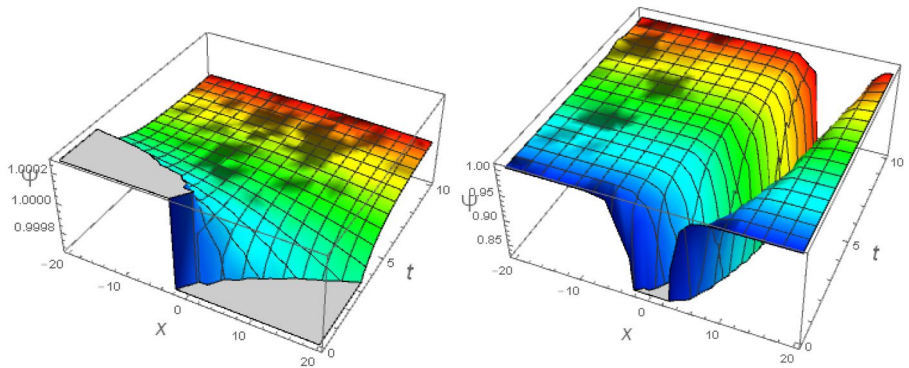
(c) 3D delineation for M-truncated operator at $\varpi = 0.1$.

(d) 3D delineation for conformable operator at $\varpi = 0.5$.

(e) 3D delineation for β-operator at $\varpi = 0.5$.

(f) 3D delineation for M-truncated operator at $\varpi = 0.5$.

Fig. 4 3D portraying for Ψ_{36} with the disparity of fractional operators and fractional order

Figure 5: Chronicle the 3D and 2D graphic comparison of dissimilar fractional differential operators for Ψ_{36} at the variation of fractional order along with practicable parametric values such as, $\rho = e$, $\kappa_1 = 1$, $\kappa_2 = 1$, $b_1 = 1$, $b_2 = 1$, $v_2 = 1$ and $\varrho = 1$.
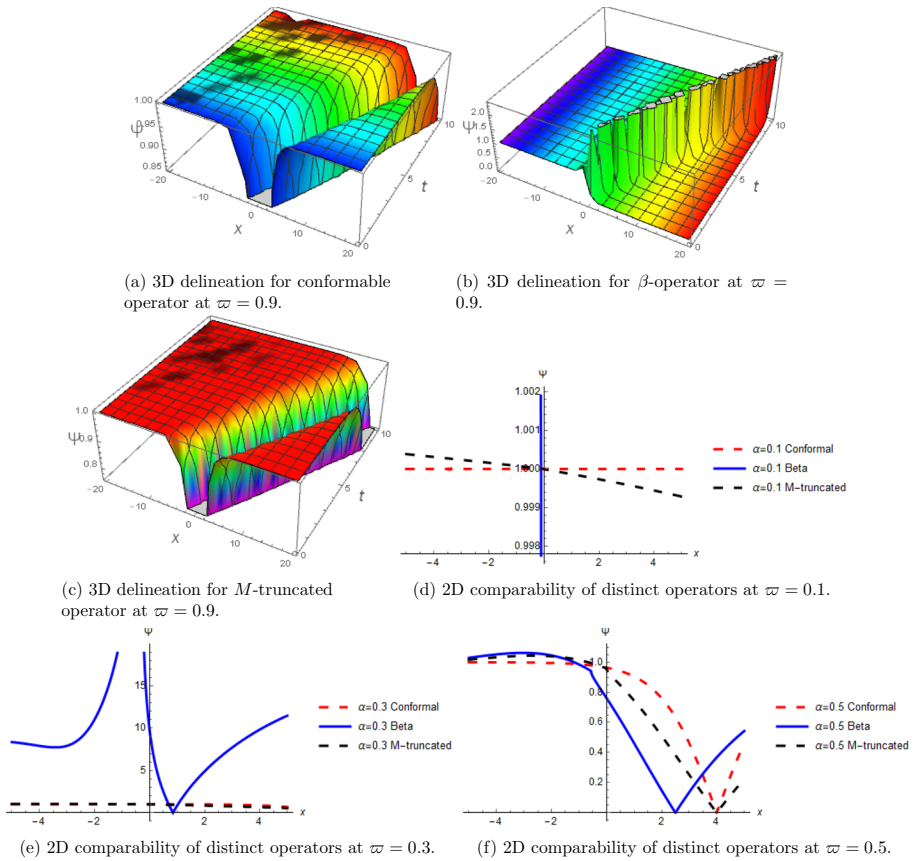
(a) 3D delineation for conformable operator at $\varpi = 0.9$.

(b) 3D delineation for β-operator at $\varpi = 0.9$.

(c) 3D delineation for M-truncated operator at $\varpi = 0.9$.

(d) 2D comparability of distinct operators at $\varpi = 0.1$.

(e) 2D comparability of distinct operators at $\varpi = 0.3$.

(f) 2D comparability of distinct operators at $\varpi = 0.5$.

Fig. 5 2D and 3D portraying for Ψ_{36} with the disparity of fractional operators and fractional order

Figure 5a–c yields 3D illustration at $\varpi = 0.9$ concerning to conformable operator, $\beta-$ fractional definition and truncated M-fractional derivative respectively.

On the account of 3D analysis, as we move towards integer order then conformable and truncated M-fractional definitions rendering almost symmetrical curve with little bit difference, however, β fractional derivative interprets a prominent variance rather than conformable and truncated M-fractional operator.

Figure 5d capitulate 2D comparision of utilized fractional definitions at $\varpi = 0.1$, Fig. 5e remit 2D comparision of executed fractional definitions at $\varpi = 0.3$, and Fig. 5f permit 2D comparision of exploited fractional definitions at $\varpi = 0.5$.

On the whole 2D inspection, the conformable and truncated M-fractional definitions manifesting almost the same pattern with little bit difference, however, β fractional derivative interprets a prominent variance rather than β and truncated M-fractional operator.

Figure 6: Represent the 2D graphic comparison of dissimilar fractional differential operators for Ψ_{36} at the variation of fractional order along with practicable parametric values such as, $\rho = e$, $\kappa_1 = 1$, $\kappa_2 = 1$, $b_1 = 1$, $b_2 = 1$, $v_2 = 1$ and $\varrho = 1$.
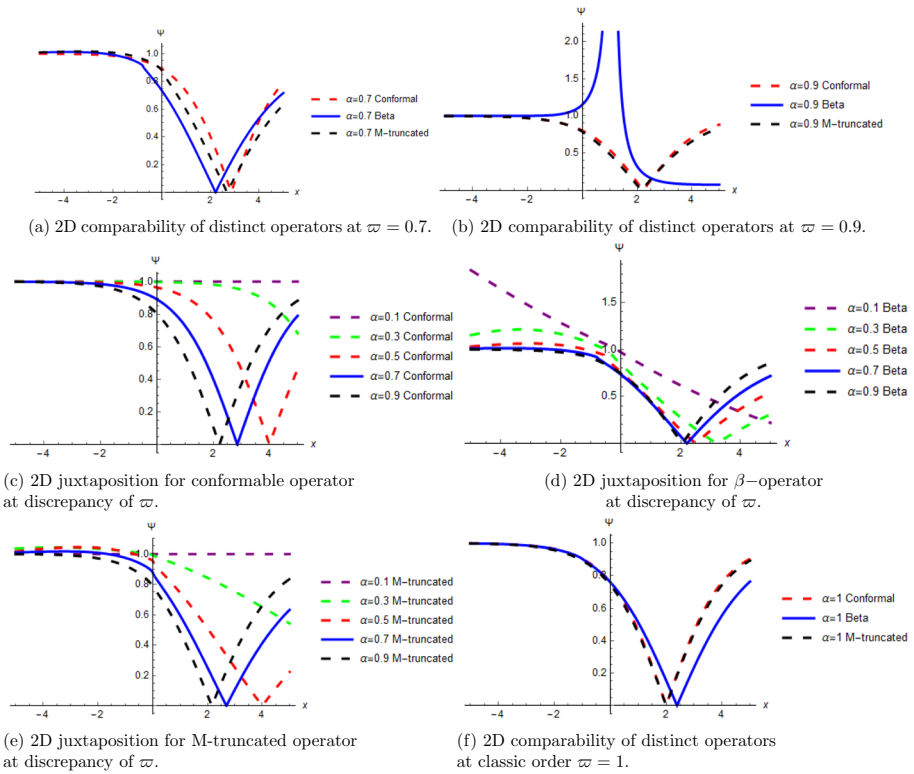
(a) 2D comparability of distinct operators at $\varpi = 0.7$.

(b) 2D comparability of distinct operators at $\varpi = 0.9$.

(c) 2D juxtaposition for conformable operator at discrepancy of ϖ.

(d) 2D juxtaposition for β−operator at discrepancy of ϖ.

(e) 2D juxtaposition for M-truncated operator at discrepancy of ϖ.

(f) 2D comparability of distinct operators at classic order $\varpi = 1$.

Fig. 6 2D portraying for Ψ_{36} with the disparity of fractional operators and fractional order and also comparision at classic order

Figure 6a capitulate 2D comparision of utilized fractional definitions at $\varpi = 0.1$, Fig. 6b remit 2D comparision of executed fractional definitions at $\varpi = 0.3$ and display the same locus as described above for 2D in Fig. 2.

Figure 6c contribute 2D comparision for conformable operator by varying fractional order, Fig. 6d contribute 2D comparision for β operator by varying fractional order, and Fig. 6e contribute 2D comparision for truncated M-fractional operator by varying fractional order.

Figure 6f delineates the comparison of prosecuted operators at classical order of derivative, which presents the efficiency of operators.

Entirely, when we analyzed all fractional 2D presentations against a single solution from the perspective of classical 2D presentation, thus we concluded that fractional study interprets deep knowledge of natural phenomenon rather than classical theory.

Remark The solution Ψ_{36} is displaying the dark-singular and kink-periodic- singular soliton solution as the fractional order increasing towards classical order.The β fractional operator demonstrate the disparate behavior compare to conformable and truncated M-fractional derivative.
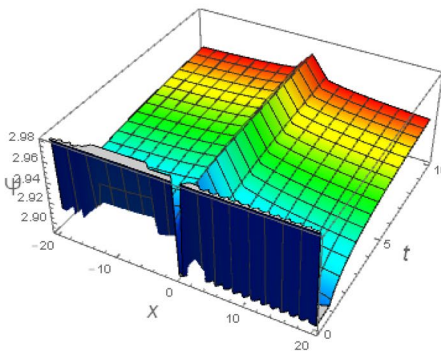
Figure 7: Depicts the 3D graphic comparison of dissimilar fractional differential operators for Ψ_{37} at the variation of fractional order along with practicable parametric values such as, $\rho = e$, $\kappa_1 = 1$, $\kappa_2 = 1$, $b_1 = 1$, $b_2 = 1$, $p = q = 1$ and $\varrho = 1$.
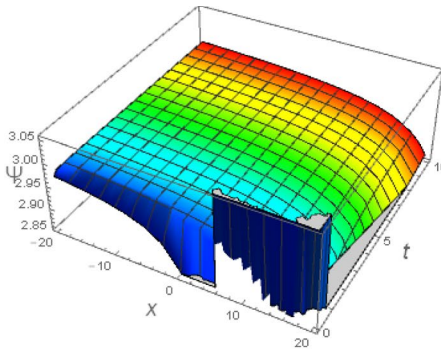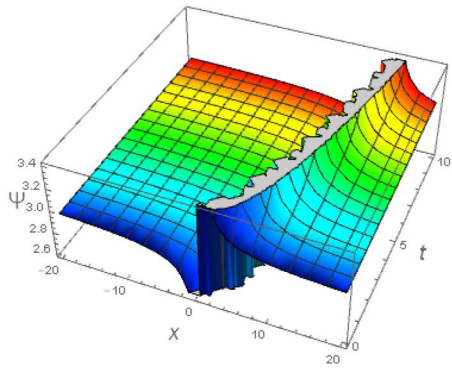

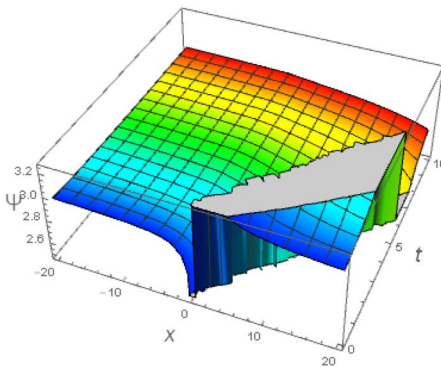(a) 3D delineation for conformable operator at $\varpi = 0.1$.
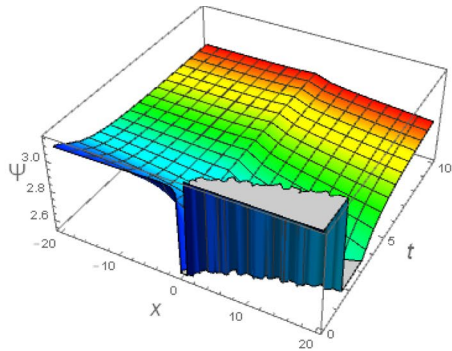
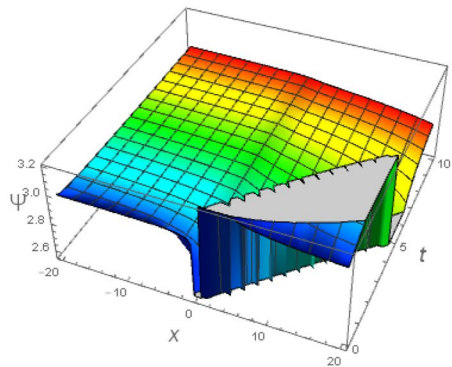(b) 3D delineation for β-operator at $\varpi = 0.1$.

(c) 3D delineation for M-truncated operator at $\varpi = 0.1$.

(d) 3D delineation for conformable operator at $\varpi = 0.5$.

(e) 3D delineation for β-operator at $\varpi = 0.5$.

(f) 3D delineation for M-truncated operator at $\varpi = 0.5$.

Fig. 7 3D portraying for Ψ_{37} with the disparity of fractional operators and fractional order

Figure 7a–c yields 3D illustration at $\varpi = 0.1$ concerning to conformable operator, $\beta-$ fractional definition and truncated M-fractional derivative respectively.

Figure 7d–f yields 3D illustration at $\varpi = 0.5$ concerning to conformable operator, $\beta-$ fractional definition and truncated M-fractional derivative respectively.

On the account of analysis, the conformable , β and truncated M-fractional definitions rendering almost distinct pattern.

Figure 8: Chronicle the 3D and 2D graphic comparison of dissimilar fractional differential operators for Ψ_{37} at the variation of fractional order along with practicable parametric values such as, $\rho = e$, $\kappa_1 = 1$, $\kappa_2 = 1$, $b_1 = 1$, $b_2 = 1$, $p = q = 1$ and $\varrho = 1$.

Figure 8a–c yields 3D illustration at $\varpi = 0.9$ concerning to conformable operator, $\beta-$ fractional definition and truncated M-fractional derivative respectively.

On the account of 3D analysis, conformable , β and truncated M-fractional definitions rendering almost symmetrical curve with little bit difference.

Figure 8d capitulate 2D comparision of utilized fractional definitions at $\varpi = 0.1$, Fig. 8e remit 2D comparision of executed fractional definitions at $\varpi = 0.3$, and Fig. 8f permit 2D comparision of exploited fractional definitions at $\varpi = 0.5$.
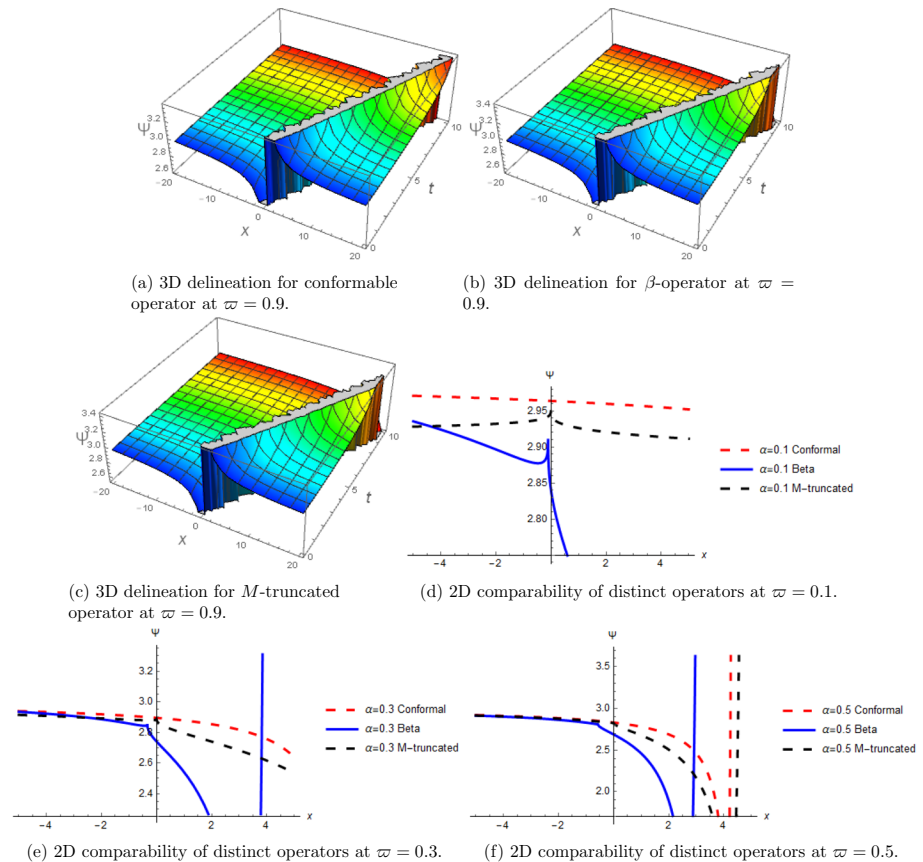

(a) 3D delineation for conformable operator at $\varpi = 0.9$.

(b) 3D delineation for β-operator at $\varpi = 0.9$.

(c) 3D delineation for M-truncated operator at $\varpi = 0.9$.

(d) 2D comparability of distinct operators at $\varpi = 0.1$.

(e) 2D comparability of distinct operators at $\varpi = 0.3$.

(f) 2D comparability of distinct operators at $\varpi = 0.5$.

Fig. 8 2D and 3D portraying for Ψ_{37} with the disparity of fractional operators and fractional order

On the whole 2D inspection, the conformable , β and truncated M-fractional definitions manifesting almost the different pattern with little bit difference.

Figure 9: Represent the 2D graphic comparison of dissimilar fractional differential operators for Ψ_{37} at the variation of fractional order along with practicable parametric values such as, $\rho = e$, $\kappa_1 = 1$, $\kappa_2 = 1$, $b_1 = 1$, $b_2 = 1$, $p = q = 1$ and $\varrho = 1$.

Figure 9a capitulate 2D comparision of utilized fractional definitions at $\varpi = 0.1$, Fig. 9b remit 2D comparision of executed fractional definitions at $\varpi = 0.3$ and display the same locus as described above for 2D in Fig. 2.

Figure 9c contribute 2D comparision for conformable operator by varying fractional order, Fig. 9d contribute 2D comparision for β operator by varying fractional order, and Fig. 9e contribute 2D comparision for truncated M-fractional operator by varying fractional order.

Figure 9f delineates the comparison of prosecuted operators at classical order of derivative, which presents the efficiency of operators.

Entirely, when we analyzed all fractional 2D presentations against a single solution from the perspective of classical 2D presentation, thus we concluded that fractional study interprets deep knowledge of natural phenomenon rather than classical theory.
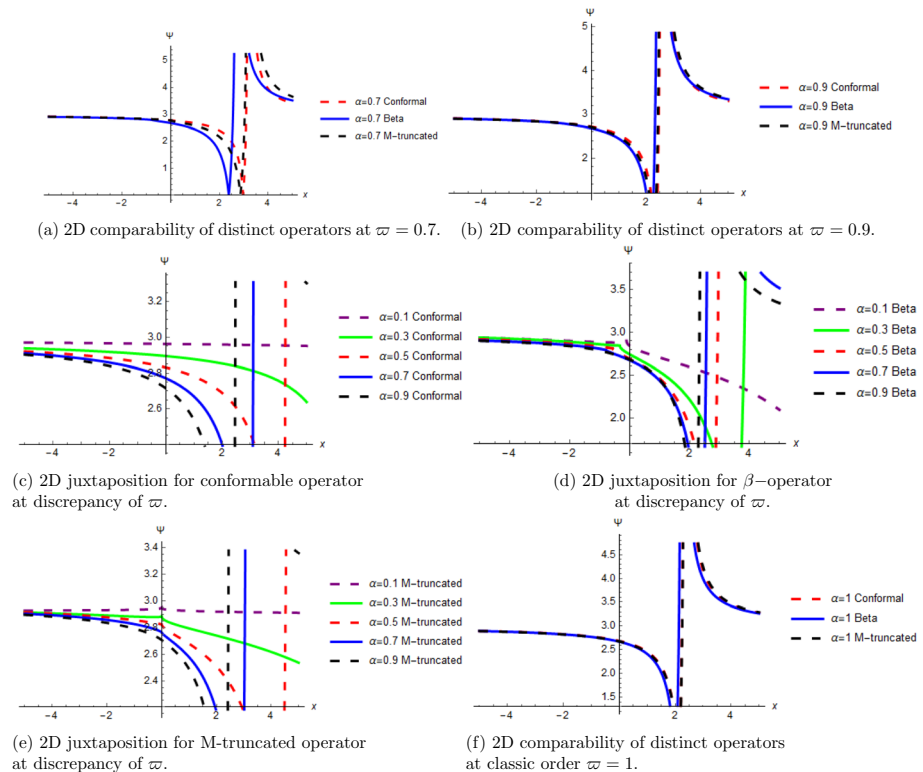

(a) 2D comparability of distinct operators at $\varpi = 0.7$.

(b) 2D comparability of distinct operators at $\varpi = 0.9$.

(c) 2D juxtaposition for conformable operator at discrepancy of ϖ.

(d) 2D juxtaposition for β−operator at discrepancy of ϖ.

(e) 2D juxtaposition for M-truncated operator at discrepancy of ϖ.

(f) 2D comparability of distinct operators at classic order $\varpi = 1$.

Fig. 9 2D portraying for Ψ_{37} with the disparity of fractional operators and fractional order and also comparision at classic order

Remark The solution Ψ_{37} is displaying the singular and bright-singular with one kink soliton solution as the fractional order increasing towards classical order. As we move far away to integer-order then conformable , *beta*, and truncated M-fractional differential operators displayed distinct behavior, however, when we take stem towards classical order, thus they try to coincide.

7 Conclusion

The non-linear elliptic Schrödinger equation is constituted in the form of a fractional partial differential equation by using the conformable operator, β operator, and truncated M-fractional derivative.The next wave traveling wave transformations have been developed to transformed PDE into ODE corresponding to considered fractional operators. The new direct extended algebraic technique has been successfully practiced to obtain solitonic structures. As result, the fractional analytical solutions such as, plane solution, mixed hyperbolic solution, periodic and mixed periodic solutions, mixed trigonometric solution, trigonometric solution, shock solution, mixed shock singular solution, mixed singular solution, complex solitary shock solution, singular solution and shock wave solutions are obtained. The acquired analytical solitary wave solutions have key applications to the optical fibers and optical communication process. An enormous study for the propagation of the pulses onward to ultra-short range in the optical communications process has been demonstrated through the fractional dynamical equation. The graphical visualization has presented of the obtained three different solutions with the assistance of `Mathematica`. The comparision of the considered fractional operators is graphically presented. The impact of fractional order is also displayed and concluded that the fractional order is responsible to control the singularity of the solutions. The effectiveness and simplicity of the utilized technique are realized from computed results. Therefore, it can be applied to other generated models in engineering and mathematics. The researchers can be explored this study furthermore in the sense of bifurcation analysis and Chaos analysis to study the phase portraits and chaotic behaviour of the model. The modulational instability gain spectrum can be developed and the sensitivity of equation can be verified by apply the sensitive analysis.

Declarations

Competing interests The authors declare that they have no competing interests.

Ethics approval and consent to participate Not applicable.

Consent for publication Not applicable.

References

Abdeljawad, T.: On conformable fractional calculus. J. Comput. Appl. Math. **1**(279), 57–66 (2015)

Adil, J., Raza, N., Rezazadeh, H., Seadawy, A.: Nonlinear self-adjointness, conserved quantities, bifurcation analysis and travelling wave solutions of a family of long-wave unstable lubrication model. Pramana **94**(1), 1–9 (2020)

Agrawal, G. P.: Nonlinear Fiber Optics. 5th ed., New York (2013)

Albadarneh, R.B., Alomari, A.K., Tahat, N., Batiha, I.M.: Analytic solution of nonlinear singular BVP with multi-order fractional derivatives in electrohydrodynamic flows. TWMS J. Appl. Eng. Math. **11**(4), 1125–1137 (2021)

Aleksei, S., Zakharov, V.: Exact theory of two-dimensional self-focusing and one-dimensional self-modulation of waves in nonlinear media. Sov. Phys. JETP **34**(1), 62 (1972)

Ali, K., Tozar, A., Tasbozan, O.: Applying the new extended direct algebraic method to solve the equation of obliquely interacting waves in shallow waters. J. Ocean Univ. China **19**(4), 772–780 (2020)

Alwyn, S.: Encyclopedia of Nonlinear Science. Routledge, New York (2006)

Atangana, A., Baleanu, D.: New fractional derivative without nonlocal and nonsingular kernel: theory and application to heat transfer model. Therm. Sci. **20**, 763–769 (2016)

Batiha, I.M., Ouannas, A., Albadarneh, R., Al-Nana, A.A., Momani, S.: Existence and uniqueness of solutions for generalized Sturm–Liouville and Langevin equations via Caputo-Hadamard fractional-order operator. Eng. Comput. (2022)

Behzad, G., Kumar, D., Singh, J.: Exact solutions of local fractional longitudinal wave equation in a magneto-electro-elastic circular rod in fractal media. Indian J. Phys. **96**(3), 787–794 (2022)

Blandford, R.D., Mitchell, C.B., Martin, J.R.: Cosmic jets. Sci. Am. **246**(5), 124–143 (1982)

Chandrasekhar, S.: Hydromagnetic Stability. Oxford University Press, Oxford (1961)

De-Jin, W., Huang, G.L., Wang, D.Y., Fälthammar, C.G.: Solitary kinetic Alfvén waves in the two-fluid model. Phys. Plasmas **3**(8), 2879–2884 (1996)

Ebenezer, B., Sagoe, A.K., Kumar, D., Deniz, S.: Fractional optimal control dynamics of coronavirus model with Mittag-Leffler law. Ecol. Complex. **45**, 100880 (2021)

Engui, F.: Extended tanh-function method and its applications to nonlinear equations. Phys. Lett. A **277**(4–5), 212–218 (2000)

Fairouz, T., Aliyu, A.I., Yusuf, A., Inc, M.: Dynamics of solitons to the ill-posed Boussinesq equation. Eur. Phys. J. Plus **132**(3), 1–9 (2017)

George W., Kumei, Sukeyuki.: Symmetries and differential equations. Vol. 81. Springer Science & Business Media (2013)

Guy, J.: Modified Riemann–Liouville derivative and fractional Taylor series of nondifferentiable functions further results. Comput. Math. Appl. **51**(9–10), 1367–1376 (2006)

Hai-Ping, Z., Pan, Z.H.: Combined Akhmediev breather and Kuznetsov–Ma solitons in a two-dimensional graded-index waveguide. Laser Phys. **24**(4), 045406 (2014)

Hamood, U.R., Imran, M.A., Bibi, M., Riaz, M., Akgül, A.: New soliton solutions of the 2D-chiral nonlinear Schrodinger equation using two integration schemes. Math. Methods Appl. Sci. **44**(7), 5663–5682 (2021)

Hamood-Ur, R., Imran, M.A., Ullah, N., Akgül, A.: Exact solutions of (2+ 1)-dimensional Schrödinger's hyperbolic equation using different techniques. Numer. Methods Partial Differ. Equ. (2020)

Hasan, N.A., Saric, W.S.: Non-linear kelvin–helmholtz instability. J. Fluid Mech. **46**(2), 209–231 (1971)

Helal, M.A., Seadawy, A.R.: Variational method for the derivative nonlinear Schrödinger equation with computational applications. Phys. Scr. **80**(3), 035004 (2009)

Holback, B., Jansson, S.E., Ahlen, L., Lundgren, G., Lyngdal, L., Powell, S., Meyer, A.: The Freja wave and plasma density experiment. The Freja Mission 173–188 (1994)

Inc, M., Yusuf, A., Aliyu, A.I., Baleanu, D.: Optical soliton solutions for the higher-order dispersive cubic-quintic nonlinear Schrödinger equation. Superlatt. Microstruct. **112**, 164–179 (2017)

Inc, M., Yusuf, A., Aliyu, A.I.: Dark optical and other soliton solutions for the three different nonlinear Schrödinger equations. Opt. Quant. Electron. **49**(11), 1–18 (2017)

Inc, M., Aliyu, A.I., Yusuf, A.: Traveling wave solutions and conservation laws of some fifth-order nonlinear equations. Eur. Phys. J. Plus **132**(5), 1–16 (2017)

Jagdev, S.: Analysis of fractional blood alcohol model with composite fractional derivative. Chaos, Solitons Fractals **140**, 110127 (2020)

Jagdev, S., Gupta, A., Baleanu, D.: On the analysis of an analytical approach for fractional Caudrey–Dodd–Gibbon equations. Alex. Eng. J. **61**(7), 5073–5082 (2022)

Kant, R., Malik, S.K.: Nonlinear waves in superposed fluids. Astrophys. Space Sci. **86**(2), 345–360 (1982)

Khater, A.H., Callebaut, D.K., Malfliet, W., Seadawy, A.R.: Nonlinear dispersive Rayleigh–Taylor instabilities in magnetohydrodynamic flows. Phys. Scr. **64**(6), 533 (2001)

Khater, A.H., Callebaut, D.K., Seadawy, A.R.: Kelvin–Helmholtz instability in MHD flows. Proc. Int. Astron. Union **2**(S233), 313–315 (2006)

Kimeu, J.M.: Fractional calculus: definitions and applications (2009)

Lindqvist, P.A., Marklund, G.T., Blomberg, L.G.: Plasma characteristics determined by the Freja electric field instrument. Space Sci. Rev. **70**(3), 593–602 (1994)

Michael, D.H.: The stability of a combined current and vortex sheet in a perfectly conducting fluid. Math. Proc. Camb. Philos. Soc. Cambridge University Press **51**(3), 528–532 (1955)

Michele, C.: Linear models of dissipation whose Q is almost frequency independent-II. Geophys. J. Int. **13**(5), 529–539 (1967)

Michele, C., Fabrizio, M.: A new definition of fractional derivative without singular kernel. Progress Fraction. Differ. Appl. **1**(2), 73–85 (2015)

Min, K., Kim, T., Lee, H.: Effects of magnetic reconnection in the Kelvin–Helmholtz instability at the magnetospheric boundary. Planet. Space Sci. **45**(4), 495–510 (1997)

Mingliang, W., Li, X.: Applications of F-expansion to periodic wave solutions for a new Hamiltonian amplitude equation. Chaos, Solitons Fractals **24**(5), 1257–1268 (2005)

Mohamed, A.Q.M., Yusuf, A., Aliyu, A.I., Inc, M.: Optical and other solitons for the fourth-order dispersive nonlinear Schrödinger equation with dual-power law nonlinearity. Superlatt. Microstruct. **105**, 183–197 (2017)

Muhammad, A., Seadawy, A.R., Lu, D.: Modulation stability and optical soliton solutions of nonlinear Schrödinger equation with higher order dispersion and nonlinear terms and its applications. Superlatt. Microstruct. **112**, 422–434 (2017)

Mustafa, I., Yusuf, A., Aliyu, A.I., Baleanu, D.: Dark and singular optical solitons for the conformable space-time nonlinear Schrödinger equation with Kerr and power law nonlinearity. Optik **162**, 65–75 (2018)

Nauman, R., Jhangeer, A., Rezazadeh, H., Bekir, A.: Explicit solutions of the (2+1)-dimensional Hirota–Maccari system arising in nonlinear optics. Int. J. Mod. Phys. B **33**(30), 1950360 (2019)

Nauman, R., Seadawy, A.R., Jhangeer, A., Butt, A.R., Arshed, S.: Dynamical behavior of micro-structured solids with conformable time fractional strain wave equation. Phys. Lett. A **384**(27), 126683 (2020)

Nauman, R., Arshed, S., Javid, A.: Optical solitons and stability analysis for the generalized second-order nonlinear Schrödinger equation in an optical fiber. Int. J. Nonlinear Sci. Numer. Simul. **21**(7–8), 855–863 (2020)

Nawaz, B., Ali, K., Rizvi, S.T.R., Younis, M.: Soliton solutions for quintic complex Ginzburg–Landau model. Superlatt. Microstruct. **110**, 49–56 (2017)

Nielsen, A.H., Pécseli, H.L., Rasmussen, J.J.: Vortex structures generated by the electrostatic Kelvin–Helmholtz instability. Ann. Geophys. **10**(9), 655–667 (1992)

Parhi, S.: A sufficient criterion for Kelvin–Helmholtz instability in the magnetopause boundary-layer region. Phys. Fluids B **4**(6), 1589–1596 (1992)

Parker, E.N.: Interplanetary Dynamical Processes (New York: Interscience). Space Sci **13**(9) (1963)

Roger, D., Faddeev, L.D., Takhtajan, L.A.: Hamiltonian methods in the theory of solitons. Bull. New Ser. Am. Math. Soc. **19**(2), 565–568 (1988)

Roshdi, K., Horani, M.A., Yousef, A., Sababheh, M.: A new definition of fractional derivative. J. Comput. Appl. Math. **264**, 65–70 (2014)

Schilinski, A.Y., Chernii, G.G.: Nonlinear Wave Processes. Mir, Moscow (1987)

Seadawy, A.R.: Approximation solutions of derivative nonlinear Schrödinger equation with computational applications by variational method. Eur. Phys. J. Plus **130**(9), 1–10 (2015)

Seadawy, A.R., Arshad, M., Dianchen, L.: The weakly nonlinear wave propagation theory for the Kelvin–Helmholtz instability in magnetohydrodynamics flows. Chaos, Solitons Fractals **139**, 110141 (2020)

Shatnawi, M.T., Ouannas, A., Bahia, G., Batiha, I.M., Grassi, G.: The optimal homotopy asymptotic method for solving two strongly fractional-order nonlinear benchmark oscillatory problems. Mathematics **9**(18), 2218 (2021)

Sousa, J. V. D. C., Oliveira, E.C.D.: A new truncated *M*-fractional derivative type unifying some fractional derivative types with classical properties (2017). arXiv preprint arXiv:1704.08187

Temerin, M., Woldorff, M., Mozer, F.S.: Nonlinear steepening of the electrostatic ion cyclotron wave. Phys. Rev. Lett. **43**(26), 1941 (1979)

Wang, Z., Pritchett, P.L., Ashour-Abdalla, M.: Kinetic effects on the velocity-shear-driven instability. Phys. Fluids B **4**(5), 1092–1101 (1992)

Weitian, Y., Liu, W., Triki, H., Zhou, Q., Biswas, A.: Phase shift, oscillation and collision of the anti-dark solitons for the (3+ 1)-dimensional coupled nonlinear Schrödinger equation in an optical fiber communication system. Nonlinear Dyn. **97**(2), 1253–1262 (2019)

Xiaoyan, L., Liu, W., Triki, H., Zhou, Q., Biswas, A.: Periodic attenuating oscillation between soliton interactions for higher-order variable coefficient nonlinear Schrödinger equation. Nonlinear Dyn. **96**(2), 801–809 (2019)

Xue, G., Liu, W., Zhou, Q., Biswas, A.: Darboux transformation and analytic solutions for a generalized super-NLS-mKdV equation. Nonlinear Dyn. **98**(2), 1491–1500 (2019)

Authors and Affiliations

Waqas Ali Faridi[1] · Muhammad Imran Asjad[1] · Adil Jhangeer[2] · Abdullahi Yusuf[3,4] · Tukur Abdulkadir Sulaiman[3,4]

[1]   Department of Mathematics, University of Management and Technology, Lahore, Pakistan

[2]   Department of Mathematics, Namal Institute, Talagang Road, Mianwali 42250, Pakistan

[3]   Department of Computer Engineering, Biruni University, Istanbul, Turkey

[4]   Department of Computer Science and Mathematics, Lebanese American University, Beirut, Lebanon